C Journal of Carbon Research

MDPI

Article

Chemical Production of Graphene Oxide with High Surface Energy for Supercapacitor Applications

Mehdi Karbak [1,2], Ouassim Boujibar [1,*], Sanaa Lahmar [1], Cecile Autret-Lambert [3], Tarik Chafik [2] and Fouad Ghamouss [1,4]

[1] Laboratory of Physical-Chemistry of Materials and Electrolytes for Energy (PCM2E), University of Tours, 37200 Tours, France; mehdi7karbak@gmail.com (M.K.); sanaa.lahmar@etu.univ-tours.fr (S.L.); fouad.ghamouss@um6p.ma (F.G.)
[2] Laboratory of Chemical Engineering and Resources Valorization (LGCVR), Faculty of Sciences and Techniques, University Abdelmalek Essaadi, B.P. 416, Tangier 90010, Morocco; tchafik@uae.ac.ma
[3] Materials Research Group, Microelectronics, Acoustics and Nanotechnologies, GREMAN, (UMR 7347), University of Tours, 37200 Tours, France; autret@univ-tours.fr
[4] Department of Materials Science, Energy, and Nano-Engineering, Mohamed VI Polytechnic University, Ben Guerir 43150, Morocco
* Correspondence: mailto:ouassim.boujibar@univ-tours.fr; Tel.: +33-7-64-77-23-88

Abstract: The chemical exfoliation of graphite to produce graphene and its oxide is undoubtedly an economical method for scalable production. Carbon researchers have dedicated significant resources to developing new exfoliation methods leads to graphene oxides with high quality. However, only a few studies have been dedicated to the effect of the starting graphite material on the resulting GO. Herein, we have prepared two different GOs through chemical exfoliation of graphite materials having different textural and structural characteristics. All samples have been subjected to structural investigations and comprehensive characterizations using Raman, X-ray diffraction, scanning electron microscopy, TGA, N_2 physisorption, and FTIR spectroscopy. Our results provide direct evidence of how the crystallite size of the raw graphite affects the oxidation degree, surface functionality, and sheet size of the resulting GO. Building on these significant understandings, the optimized GO achieves a highly specific capacitance of 191 $F \cdot g^{-1}$ at the specific current of 0.25 $A \cdot g^{-1}$ in an aqueous electrolyte. This superior electrochemical performance was attributed to several factors, among which the specific surface area was accessible to the electrolyte ions and oxygenated functional groups on the surface, which can significantly modify the electronic structure of graphene and further enhance the surface energy.

Keywords: graphene oxide; graphene; graphite; supercapacitor

Citation: Karbak, M.; Boujibar, O.; Lahmar, S.; Autret-Lambert, C.; Chafik, T.; Ghamouss, F. Chemical Production of Graphene Oxide with High Surface Energy for Supercapacitor Applications. *C* **2022**, *8*, 27. https://doi.org/10.3390/c8020027

Academic Editors: Giuseppe Cirillo and Peter Harris

Received: 2 March 2022
Accepted: 5 May 2022
Published: 7 May 2022

1. Introduction

Today, many ongoing studies are focusing on every possible type of advanced energy storage device, including alkali metal-ion batteries, fuel cells, and supercapacitors [1–3]. The latter are considered among the most promising devices due to related high power densities and a long cyclic life [4]. Generally, electrodes with a large surface area and a well-designed pore size distribution are found to be responsible for the excellent capacitive performance of supercapacitors [5]. A remarkable number of different types of carbon materials, such as activated carbon, graphene, carbon nanotubes, and carbon nanofibers, have been investigated to check their performances as electrodes for supercapacitor applications [6–8]. Among them, two-dimensional graphene-like sheets have recently received rapidly growing attention in supercapacitors, mainly because of their highly specific surface area (~2600 $m^2 \cdot g^{-1}$), superior electrical conductivity, and excellent chemical stability [9,10]. However, when graphene layers are assembled into a supercapacitor electrode, the unavoidable aggregation of graphene nanosheets and their strong π–π interactions will eventually

cause a compact restack of the atomic layers, which restricts the diffusion of electrolyte ions between graphene layers [11]. Consequently, the capacitance of the graphene inevitably decreases far below its theoretical value (21 $\mu F \cdot cm^2$). Recently, there has been an increasing amount of research into graphene oxide (GO), which exhibits higher capacitance than graphene due to the presence of oxygen-containing functional groups on its basal planes and at its edges such as epoxy, carbonyl, and carboxyl groups [12]. The presence of these oxygen functionalities in GO participates in redox reactions and thus contributes to an additional pseudo-capacitance.

GO can be obtained by chemical oxidative exfoliating of graphite powder, which is the most widely used method for graphene preparation due to its low cost, facile preparation process and significant productivity [13]. In oxidation–exfoliation, GO synthesis normally begins by intercalating a strong oxidant and concentrated acidic solution to oxidize the graphite material. The most popular methods for GO were the Hummer's method and modified Hummer's method, which use the mixture of potassium permanganate ($KMnO_4$) and sulfuric acid (H_2SO_4) [14,15]. In addition, many efforts have been made recently to optimize the preparation methods, but the protocols developed are not significantly different from the initial Hummer's method [16–19]. However, even though GO is being fabricated using the modified Hummers method, the experimental conditions differ for each research group, and the physical and chemical structures of the GO vary significantly.

Besides, the structural and textural properties of graphite used as a precursor are also considered key parameters governing the production of high-quality GO. Many studies have investigated the influence of the particle size of the precursor graphite on the GO structure by using graphites with different particle and crystallite sizes [20,21] as precursors. It was found that the graphites with a large crystallite size led to the formation of a GO with a high proportion of hydroxyl (–OH) and epoxy (C–O–C) groups located at the plane, whereas oxidation at the sheet edges was dominant for graphites with smaller crystallites [20]. Furthermore, large and nonuniform graphite flakes made oxidation very difficult by limiting the reactant diffusion inside the crystallite [22]. Therefore, several methods have been proposed to improve this diffusion [23,24]. Recently, Yuhang Liu and his colleagues showed that adding ammonium persulfate ($(NH_4)_2S_2O_8$) to concentrated sulfuric acid as a gas expansion agent enables the expansion of the graphite structure, which improves its specific surface area and, therefore, allows for the penetration of oxidizing agents [25]. This approach has been adopted in the present work and yields GOs from graphite with different crystallite sizes. The key objective in the present work is to explore and establish the influence of the structural and textural properties of graphite materials on the physical-chemical properties of graphene oxides. The as-prepared GOs are investigated with respect to potential application as electrodes for supercapacitor applications. The properties of the synthesized GOs are extensively studied and compared to understand the effect of structural and textural properties of the graphite. The electrochemical performance of GOs is also evaluated in an aqueous electrolyte. The obtained results are discussed and compared with respect to other cutting-edge research results.

2. Materials and Methods

2.1. Chemicals

KS6 (S-231) and SFG6 (R-154) graphite flakes were purchased from TIMCAL group Ltd. Potassium permanganate ($KMnO_4$, AR, $\geq$99%), sodium nitrate ($NaNO_3$, AR, $\geq$99%), concentrated sulfuric acid (H_2SO_4, AR, 96%), and hydrogen peroxide (H_2O_2) were obtained from SIGMA ALDRICH. Ammonium persulfate ($(NH_4)_2S_2O_8$, 98%) was purchased from Alfa Aesar. All reagents were used as received without any further treatment.

2.2. Materials Synthesis

In a round bottom flask, 2 g of graphite (KS6 or SFG6) was dispersed in 80 mL concentrated sulfuric acid using a magnetic stirrer at 30 °C. After 10 min, 20 g of ammonium persulfate $(NH_4)_2S_2O_8$ was added to the graphite suspension and stirred for 2 h to obtain

an expanded graphite. The gas expansion process was followed by adding another 120 mL of concentrated sulfuric acid. The mixture was transferred into an ice water bath to ensure a temperature below 5 °C. One gram of sodium nitrate was added to the mixture; subsequently, 16 g of potassium permanganate was equally divided into 6 parts and added every 10 min. The mixture was placed in a 35 °C water bath and stirred for 2 h. Then, 400 mL of distilled water was added dropwise, and therefore graphene oxide was acquired. Once the temperature decreased to 25 °C, 30 mL of hydrogen peroxide was added into the mixture to reduce the unreacted potassium permanganate until a yellowish suspension was obtained. The mixture was filtered and washed under vacuum with distilled water until the filtrate reached a neutral pH. The obtained material was dried in a 100 °C oven for 24 h and ground by an agate mortar. The final product is denoted GO-KS6 (graphene oxide KS6) and GO-SFG6 (graphene oxide SFG6), respectively, originating from graphite sources KS6 and SFG6.

2.3. Materials Characterization

To understand the structural and textural implications of graphite on the synthesis of an ideal graphene oxide, the morphologies of all samples were examined by scanning electron microscopy. RAMAN spectra were obtained using a HORIBA LabRAM HR Evolution at room temperature with an integration time of 10 s for three accumulations using a 100× objective lens and a laser source of 514 nm. The nitrogen adsorption equilibrium isotherms were obtained using a QUADRASORB EVO analyzer measured at 77 K. All samples were degassed at 353 K for 4 h under vacuum before all porosity measurements. The specific surface area (S_{BET}) was determined by the Brunauer–Emmett–Teller (BET) theory, considering the molecular cross-sectional area of N_2 at 77 K to be 0.162 nm^2 [26]. Pore size distribution and pore volume were calculated using the Quenched Solid-state Density Functional Theory (QSDFT) [27]. Crystallographic properties of all the samples were investigated by X-ray diffraction using an X-ray diffractometer D8 Discover operating at 40 kV and 40 mA using Ni-filtered Cu Kα radiation (k = 0.15406 nm). Data were recorded in the 2θ range of 15° and 70° with a step size of 0.02° and a step time of 1 s. The structural parameters included the interplanar distance (d_{002}), crystallite diameter (*La*), and crystalline height (*Lc*), which were calculated according to Equations (1)–(3), using the full-width at half-maximum values of (002) and (100) peaks [28].

$$d_{002} = \frac{\lambda}{2sin\theta} \quad (1)$$

$$L_a = \frac{K\lambda}{\beta_a cos\theta_a} \quad (2)$$

$$L_c = \frac{K\lambda}{\beta_c cos\theta_c} \quad (3)$$

where d = the interlayer spacing, θ = the diffraction angle, λ = the wavelength of the X-ray source, and β = the full peak width of the diffraction peak at half the maximum height (FWHM).

To investigate the functional groups in the all samples, PerkinElmer Spectrum Two was used for the Fourier-transforming infrared spectroscopy (FTIR) analysis. TGA experiments were performed on all the samples under the N_2 atmosphere at a flow rate of 60 mL/min and a heating rate of 5 °C·min^{-1} from 100 °C to 600 °C, using a TGA 800 PerkinElmer.

2.4. Electrochemical Characterization

For electrochemical characterization, working electrodes (Graphite KS6, Graphite SFG6, GO-KS6, or GO-SFG6) and counter electrodes (activated carbon with a large surface area) were prepared by mixing 80% active material, 10% carbon black, and 10% polytetrafluoroethylene (PTFE). The prepared paste was then kneaded into a paper-like form and dried at 60 °C for 12 h, before being pressed at 10 tones on a 10 mm of diameter stainless

steel round mesh. A 3-electrode Swagelok type cell was assembled using the prepared working electrodes (WE), the counter electrode (CE), and the saturated calomel electrode (SCE) as reference electrodes, and an electrolyte containing 0.5 M potassium sulfate (K_2SO_4) dissolved in degassed distilled water.

3. Results and Discussion

3.1. Materials Characterization

Raman spectroscopy and X-ray diffraction were used for further investigation of the crystallographic structure of the graphite samples and the as-prepared GOs. Figure 1 shows the Raman spectrum of both graphite and the synthesized GOs. All profiles were normalized by the peak of the G band appearing at 1580 $cm^{-1,}$ which originates from the vibration of ordered sp2 carbon. The D band at ~1350 cm^{-1} is attributed to the defects of graphite and the double resonant processes near the K point of the Brillouin Zone boundary [29]. The intensity ratio of the D to the G band can be used to estimate the graphitization degree of the carbon-based materials. Thus, the I_D/I_G ratio tends to increase with the reduction of the crystallite size of the graphite due to the presence of edge defects. The Raman spectra of KS6 show a higher I_D/I_G (0.37) value compared with the SFG6 (0.27), indicating that the KS6 have a smaller crystallite size. The Raman spectra of GO-KS6 and GO-SFG6 exhibit a typical graphene-like pattern. It is important that the I_D/I_G ratio of GO-KS6 (1.04) is slightly higher than the I_D/I_G ratio for GO-SFG6 (0.96), indicating that the GO-KS6 sheets have more defects in their structure. Figure 1b shows the XRD diffraction results of the graphite powders as well as the graphene oxides prepared. The XRD diffractogram of graphite materials shows the absence of any peaks attributed to the mineral phase, indicating their high purity and good graphitic structure. The graphite samples show a (002) peak near 26° and a (100) peak near 43° [30].

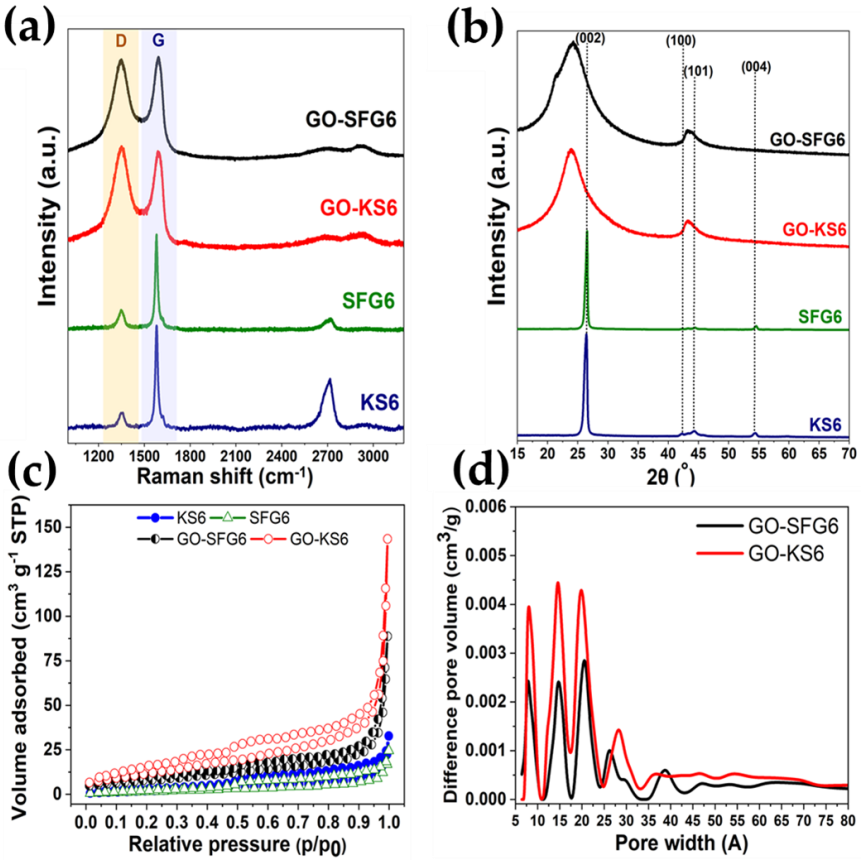

Figure 1. (**a**) The Raman spectra, (**b**) the X-ray diffraction patterns, (**c**) the N_2 adsorption isotherms, and (**d**) the pore size distribution obtained from all GOs prepared and from both graphite precursors.

As shown in Table 1, the two graphites are characterized by similar interplanar distances (∼0.30 nm). In good agreement with the results of Raman studies, SFG6 graphite presents a larger crystallite size than KS6. After the exfoliation process, the peak (002) is transferred to the range of 20 to 26°, confirming the significant presence of the sp2 domains, possibly with the off-the-plane oxygen groups. In addition, the crystallite size of GOs decreases significantly, while the interplanar distance increases. The increasing of the interplanar distance between the graphene layers of the GOs samples due to the attachment of the oxygen functional groups on the graphene nanosheet that work as spacers was confirmed by the TGA and FTIR investigations. However, the GO obtained from KS6 yielded a slightly higher d002. These features are, apparently, associated with the small crystallites size of the KS6, which is easily oxidized to form more oxygen-containing functional groups on the graphene edges. Owing to its larger crystallites size, the oxygen functional groups on GO-SFG6 mainly occur in the basal plane defects, resulting in the significant modification of the electronic structure of graphene and the further enhancement of the surface energy.

Table 1. The structural parameters of the graphite precursors and the prepared GOs.

Sample	XRD Parameters			Raman Parameters
	d_{002}(nm)	La (nm)	Lc (nm)	I_D/I_G
KS6	0.33	19.18	31.25	0.37
SFG6	0.31	20.85	40.21	0.27
GO-KS6	0.40	4.63	20.76	1.04
GO-SFG6	0.36	4.51	17.67	0.96

The textural characterization of all the samples was investigated using N_2 physisorption measured at 77 K. Figure 1c shows the isotherms obtained. Based on the International Union of Pure and Applied Chemistry (IUPAC) classification, these isotherms are characteristic of type IV and a hysteresis loop of H4 attributed to the capillary condensation of N_2 in the mesoporous structure [31]. The measured isotherms permitted the determination of textural parameters of all samples presented in Table 2. The largest S_{BET} value was obtained for GO-KS6 (50 m^2/g), while GO-SFG6 yielded a slightly reduced S_{BET} (37 m^2/g). However, the pores size distribution (PSD) derived from N_2 adsorption isotherms using the DFT method showed some porosity distribution for the two prepared GOs. The developed porosity is predominantly microporous, with some amount of mesopores, as depicted by the shoulders between 20 and 80 Å (Figure 1d). Despite lower values of BET surface aera, the electrochemical performances of the synthesized GOs will certainly depend not only on the nature of porosity but also on other parameters, such as the surface energy, the structural properties, and the electronic properties of involved surface functions.

Table 2. The textural parameters of the graphite precursors and the prepared GOs.

Sample	S_{BET}	Pore Volume (cm^3/g)			
		V_T	V_{micro}	V_{meso}	V_{micro}/V_T (%)
KS6	20	0.037	0.006	0.031	19.35
SFG6	15	0.030	0.005	0.024	20.83
GO-KS6	51	0.094	0.016	0.078	82.97
GO-SFG6	31	0.062	0.011	0.051	82.25

The morphology of the graphite samples and synthesized GOs was investigated by SEM. Figure 2a,b shows the SEM images obtained for the above graphite powders and they all exhibit a flake-like structure with sharp edges. In agreement with the XRD and Raman results, the graphite KS6 presents fine particles compared to SFG6. Furthermore, as shown

in Figure 2c,d, the GO-KS6 sample seems to present a honeycomb-like structure with large porous multi-cavities. Moreover, in contrast to the displayed smooth rifts and crannies of GO-KS6, the surface of GO-SFG6 presents randomly aggregated, thin, crumpled sheets closely associated with each other and forming a disordered solid.

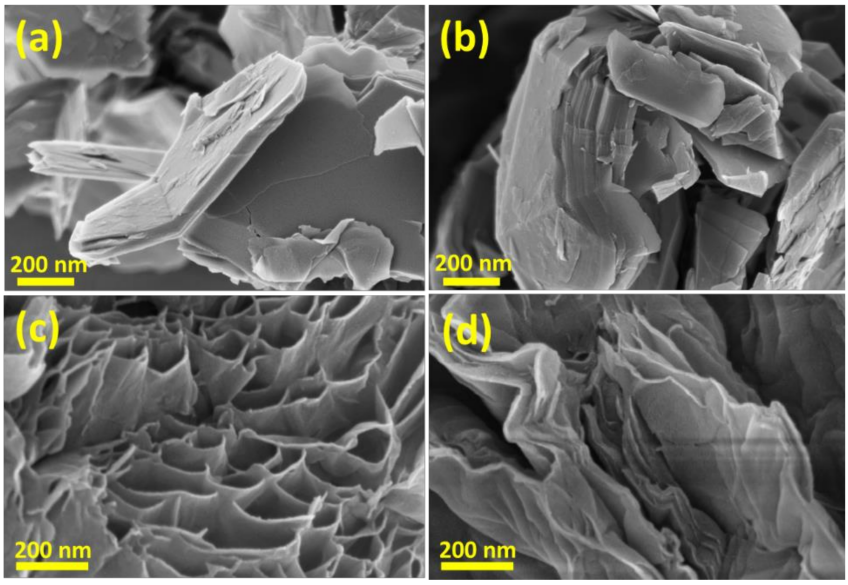

Figure 2. The SEM micrographs of the KS6 (**a**), SFG6 (**b**), GO-KS6 (**c**), and GO-SFG6 (**d**).

Thermogravimetric analyses were employed on graphite and graphene-oxide materials to glean information on oxygen functionalities. In Figure 3a, KS6 graphite does not show any weight loss even at 600 °C, counter to SFG6 graphite, which exhibits a 4% drop by losing the unstable functioning groups. On the other hand, the release of pore water trapped between GO-KS6 and GO-SFG6 sheets is expressed by a small weight drop (4% and 6%, respectively) before 100 °C. The next weight drop starts at around 160 °C and keeps going slowly and steadily until it reaches a total of 20% for GO-KS6 and 24% for GO-SFG6. The drop at low temperatures (160 °C to 380 °C) can be attributed to the elimination of the moisture and the H_2O molecules and the decomposition of unstable O_2-rich functional moieties such as alcohol, and epoxy groups [32]. At the temperatures above 400 °C, there is a general decline of the relatively stable O_2-rich moieties such as quinine, alcohol, and terminal carboxyl groups in the sp^2 hybridized c-network in GOs [33,34]. Even though graphene samples show comparable results, the oxidation level of GO-SFG6 may be higher than that of GO-KS6.

To determine the existing functional groups for each material, FTIR analysis was performed. As displayed in Figure 3b, both graphite samples (KS6 and SFG6) show no significant peaks of any functional groups, indicating the chemical inertia of commercial graphite materials. To counterbalance, GO-KS6 and GO-SFG6 show intense and steep peaks (1180 cm^{-1}, 1560 cm^{-1}, and 1720 cm^{-1}) that correspond, respectively, to the C-O-C, C=C, and C=O groups. These results confirm the presence of certain oxygen functional groups on the graphene oxide sheet structure, which is in good agreement with the TGA results. It is worth noting that the FTIR spectra of the GOs prepared do not reveal the presence of well-defined peaks that might be associated with any N-containing functional groups (3200–3700 cm^{-1}) that can be drawn from ammonium persulphate. Figure 3c shows the digital pictures of the GOs dispersion in various types of solvents. Owing to its high oxygen-containing functional groups on the surface, GO-SFG6 showed very good dispersion in water, N-methyl-2-pyrrolidinone, and acetone. These solutions are usually stable for a long period of time, depending on the concentration. However, some of the GO-KS6 particles underwent significant aggregation and precipitated to the bottom of the container, thereby resulting in a transparent solution. This is, presumably, due to a low oxidation degree

of GO-KS6 sheets because of π-π stacking interactions. By performing wettability and surface tension measurements, the contact angle of water in GO-KS6 and GO-SFG6 has been estimated to be ∼87° and ∼66°, respectively, as shown in the images of Figure 3d. Thus, the analysis of the GO materials by the contact angle was in good agreement with the results of the textural and structural characterizations. The numerous defects on the GO-SFG6 layers can potentially alter their surface energy, and that in turn enhances their surface polarity. Therefore, as-prepared GOs with higher defect densities were expected to exhibit higher electrochemical performances as electrodes for supercapacitors.

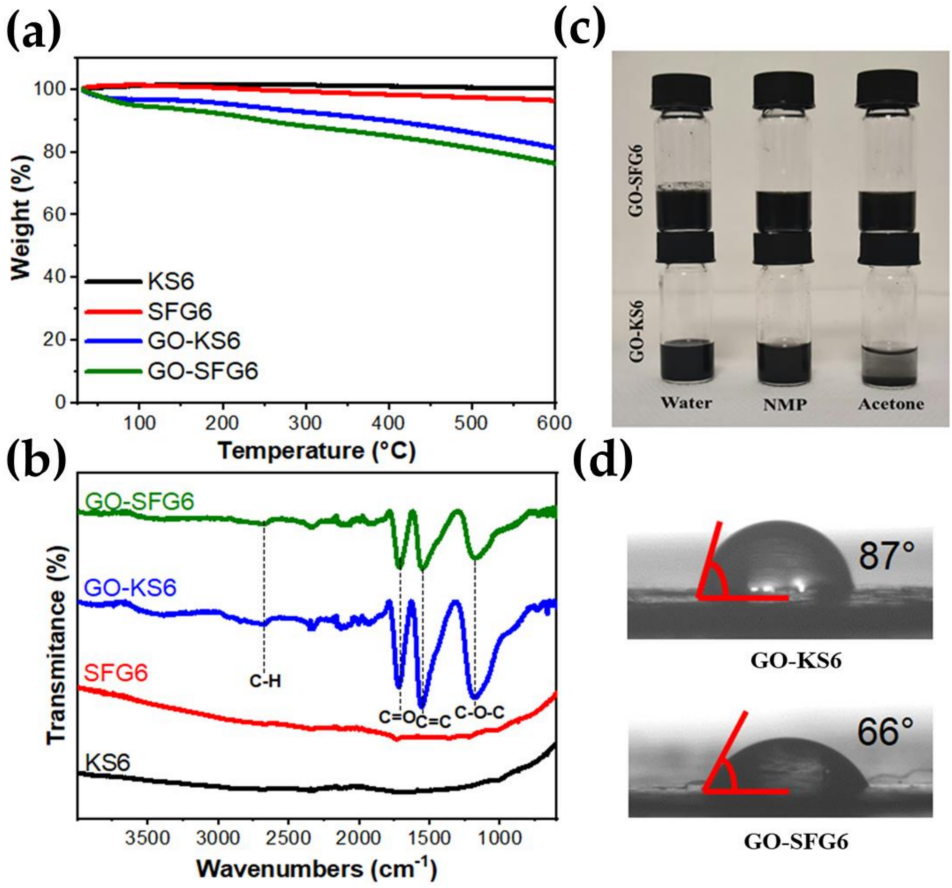

Figure 3. (**a**) The TGA profiles of all samples. (**b**) The FTIR specters of all samples. (**c**) The digital pictures of the GOs dispersions in various solvents. (**d**) The digital pictures of contact angle measurements of water in GO-KS6 and GO-SFG6 samples.

3.2. Electrochemical Properties

For a better understanding of the synthesized materials and the effect of their structural and textural properties on their capacitance to store energy, a series of electrochemical analyses were conducted on all materials by a three-electrode system in the 0.5 M K_2SO_4 electrolyte. Using cyclic voltammetry at a scan rate of 20 $mV \cdot s^{-1}$ in a voltage window between −0.9 V and 0 V versus SCE, we implemented a basic comparison between each graphite and its synthesized graphene. As shown in Figure 4a,b, both graphite samples generate a negligible specific current next to that of graphene. The specific capacitance for KS6 and SFG6 graphite is 5 $F \cdot g^{-1}$ and 6 $F \cdot g^{-1,}$ respectively. Contrastingly, the specific capacitance of GO-KS6 and GO-SFG6 is dramatically increased to 115 $F \cdot g^{-1}$ and 141 $F \cdot g^{-1}$, representing, respectively, 20 and 22 times more specific capacitance than that of starting graphite. This significant difference can be attributed to the increased specific surface area (≈2 times more surface in graphene materials than in graphite) and hence the accessible graphene pores, as well as the increased surface energy and conductivity.

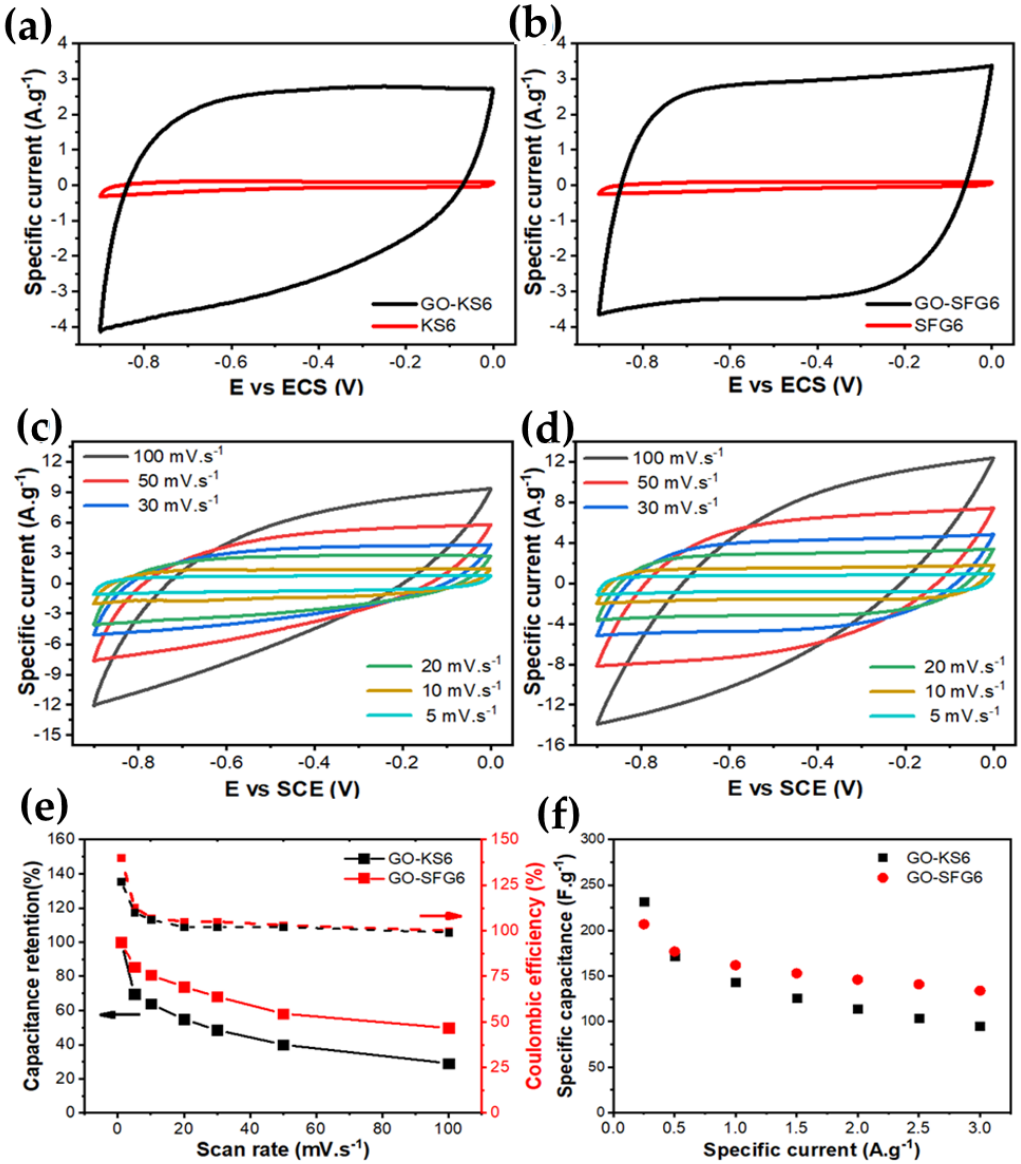

Figure 4. (**a**) The CV comparison between KS6 graphite and GO-KS6, (**b**) the CV comparison between SFG6 graphite and GO-SFG6, (**c**) the CV curves of GO-KS6 at different scan rates, (**d**) the CV curves of GO-SFG6 at different scan rates, (**e**) the capacitance retention at different scan rates, and (**f**) the specific capacitance at different specific currents in the galvanostatic charge–discharge.

Figure 4a,b also demonstrates the difference between GO-KS6 and GO-SFG6. Both materials show a nearly rectangular CV curve, indicating excellent charge capacitive and the low level of activity of the oxygen functional groups. However, GO-SFG6 distinguishes itself from GO-KS6 with a less oblique loop, representing better conductivity and a larger current density. We further studied graphene materials by implementing different scan rates, 1 mV·s^{-1} to 100 mV·s^{-1}. Using CV curves in Figure 4c,d, we calculated the specific capacitance of GO-KS6 and GO-SFG6 at different scan rates.

As shown Figure 4e, the GO-KS6 sample reached the specific capacitance value of 210 F·g^{-1} at 1 mV·s^{-1}. When the scan rate was increased, the specific capacitance decreased gradually until it reached 61 F·g^{-1} at 100 mV·s^{-1}. For GO-SFG6, even though it showed less specific capacitance than GO-KS6 (191 F·g^{-1}) at 100 mV·s^{-1}, it maintained its capacitance better, even at 100 mV·s^{-1} (95 F·g^{-1}). GO-SFG6 retained 50% of its initial specific capacitance, while GO-KS6 only kept 29%. These results confirm that GO-SFG6 has better electrochemical kinetics and can function properly even at high scan rates. Using

galvanostatic charge–discharge, we investigated the rate capability of graphene materials between 0.25 $A{\cdot}g^{-1}$ and 3 $A{\cdot}g^{-1}$. The results exhibited in Figure 4f confirm that GO-SFG6 demonstrates better electrochemical kinetics, starting with 207 $F{\cdot}g^{-1}$ at 0.25 $A{\cdot}g^{-1}$ and maintaining 134 $F{\cdot}g^{-1}$ at 3 $A{\cdot}g^{-1}$ (represents 64%), while GO-KS6 started with 232 $F{\cdot}g^{-1}$ at 0.25 $A{\cdot}g^{-1}$ and kept 95 $F{\cdot}g^{-1}$ at 3 $A{\cdot}g^{-1}$ (represents 40%). Based on the previous textural and structural characterizations, the higher electrochemical performances of the GO-SFG6 sample might be associated with the higher attractive force imparted by the related important presence of non-carbon elements, such as oxygen.

Since we have already demonstrated the effect of the electrochemical kinetics on the specific capacitance, we considered the presence of two storage mechanisms, the capacitive mechanism, and the faradic-controlled mechanism. The capacitive mechanism is known for its fast kinetics at the electrode–electrolyte interface, even at high-current densities. On the other hand, the faradic-controlled mechanism is much slower, originating from the functional groups' redox reactions. From cyclic voltammetry at different scan rates and using Dunn's method, we can quantify the contribution of both mechanisms at different kinetic properties [35]. The capacitive contribution was calculated by Dunn's method. At a fixed voltage, the capacitive current and the diffusion-controlled current can be described by Equations (4) and (5).

$$i_{cap}(v) = k_1 v \tag{4}$$

$$i_{far}(v) = k_2 v^{\frac{1}{2}} \tag{5}$$

The current measured by cyclic voltammetry is:

$$i_{CV}(v) = k_1 v + k_2 v^{\frac{1}{2}} \tag{6}$$

After we divide Equation (5) by $v^{\frac{1}{2}}$, we get

$$\frac{i_{CV}(v)}{v^{\frac{1}{2}}} = k_1 v^{\frac{1}{2}} + k_2 \tag{7}$$

By collecting $i_{cv}(v)$ from cv plots at different scan rates and plotting $\frac{i_{CV}(v)}{v^{\frac{1}{2}}}$ vs $v^{\frac{1}{2}}$, we obtained a linear equation where k_1 represents the slope and k_2 represents the intercept. Then, we could calculate the capacitive current and diffusion-controlled current.

In our calculation, we input 1000 points selected from each CV curves (−0.9 V to 0) at scan rates of 1, 5, 10, 15, 20, and 30 $mV{\cdot}s^{-1}$ for each electrode.

Faradic-controlled contribution for GO-KS6 (Figure 5) is remarkably higher than GO-SFG6; it starts at 22% for a scan rate of 30 $mV{\cdot}s^{-1}$ and increases to 63% at 1 $mV{\cdot}s^{-1}$. Considering how slow this mechanism is, it cannot deliver as much capacitance as it can in high-current densities. This explains the capacitance decay at highly specific currents. On the other hand, GO-SFG6 holds a larger capacitive contribution even at low scan rates (63% at 1 $mV{\cdot}s^{-1}$). This means that this material can work at highly specific currents because most of its capacitance is associated with a fast kinetic mechanism.

The electrochemical capacitance values obtained with the GOs prepared in our work are presented in Table 3 for the sake of comparison with the most relevant values reported in the literature for several GOs prepared by the different methods, including some reduced graphene oxide.

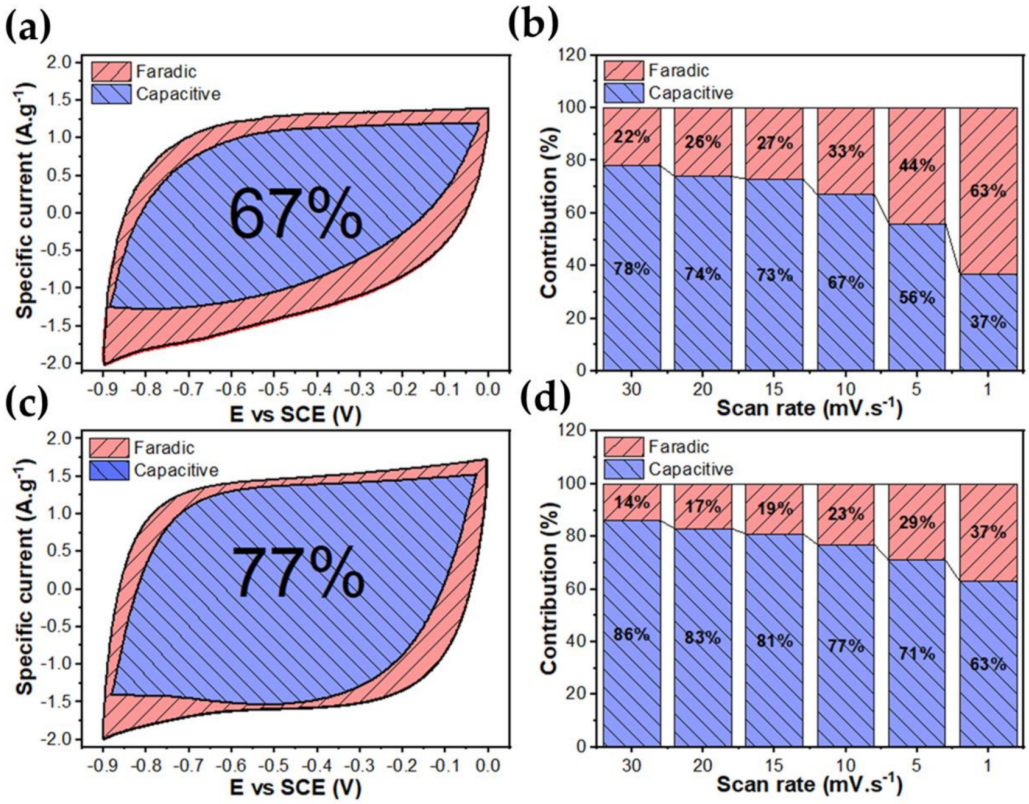

Figure 5. (**a**,**b**) The capacitive contribution of GOKS6 at different scan rates; (**c**,**d**) the capacitive contribution of GO-SFG6 at different scan rates.

Table 3. The performance comparison of GOs-based-derived electrodes under a three-electrode system in aqueous electrolytes.

Material	Electrolyte	Capacitance	References
Holey graphene	6 M KOH	190 $F \cdot g^{-1}$ at 1 $A \cdot g^{-1}$	[36]
Reduced GO	2 M KOH	212 $F \cdot g^{-1}$ at 1 $A \cdot g^{-1}$	[37]
Reduced GO	1 M Na_2SO_4	114 $F \cdot g^{-1}$ at 3 $A \cdot g^{-1}$	[38]
GO nanosheets	1 M Na_2SO_4	98.8 F/g at 0.5 mA/cm^2	[39]
Reduced GO aerogel	1 M Na_2SO_4	123 $F \cdot g^{-1}$ at 5 mV/s	[40]
Graphene Hydrogel	1 M KOH	160 $F \cdot g^{-1}$ at 1 $A \cdot g^{-1}$	[41]
GO	6 M KOH	123 $F \cdot g^{-1}$ at 5 $A \cdot g^{-1}$	[11]
GO-KS6	0.5 M K_2SO_4	143 $F \cdot g^{-1}$ at 1 $A \cdot g^{-1}$	This work
GO-SFG6	0.5 M K_2SO_4	162 $F \cdot g^{-1}$ at 1 $A \cdot g^{-1}$	This work

4. Conclusions

In summary, graphene oxides derived from two graphites were synthesized and tested as a supercapacitor electrode. The observed difference in the structural and textural properties of the graphites has enabled us to obtain two graphene oxides. So far, the experimental investigations indicated that the graphene oxide obtained from the graphite with a large crystallite size was found to present high surface energy, mainly due to its high proportion of oxygen function groups and basal plane defects, whereas the graphene oxide with the small-crystallite-sized graphite contained predominantly edge plane defects, indicating

their different chemical behavior. Further, the GO-SFG6 with a high surface energy electrode provided a superior specific capacitance of 162 $F \cdot g^{-1}$ at 1 $A \cdot g^{-1}$.These results provide direct evidence of the active role played by the structural characteristics of the parent graphite, resulting in graphene oxides with promising potential for supercapacitor applications.

Author Contributions: Writing—original draft and methodology, M.K.; methodology, S.L.; writing—review, C.A.-L.; writing—review, T.C.; writing—review, editing and project management, F.G.; and conceptualization, methodology, writing—original draft, writing—review and editing, O.B. All authors have read and agreed to the published version of the manuscript.

Funding: This work was supported by the ANR, France, under the projects "ANR-18-ASMA-0001-01S3CAP". The CNRST/Morocco is also acknowledged for its financial support through the "project PPR2/2016/17".

Institutional Review Board Statement: Not applicable.

Informed Consent Statement: Not applicable.

Data Availability Statement: Data are contained within the article.

Acknowledgments: The authors would like to thank Pierre Ivan Raynal for his help in SEM acquisition.

Conflicts of Interest: The authors declare no conflict of interest.

References

1. Goodenough, J.B.; Park, K.-S. The Li-Ion Rechargeable Battery: A Perspective. *J. Am. Chem. Soc.* **2013**, *135*, 1167–1176. [CrossRef] [PubMed]
2. Gür, T.M. Review of electrical energy storage technologies, materials and systems: Challenges and prospects for large-scale grid storage. *Energy Environ. Sci.* **2018**, *11*, 2696–2767. [CrossRef]
3. Simon, P.; Gogotsi, Y. Perspectives for electrochemical capacitors and related devices. *Nat. Mater.* **2020**, *19*, 1151–1163. [CrossRef]
4. Miller, J.R.; Simon, P. Electrochemical Capacitors for Energy Management. *Science* **2008**, *321*, 651–652. [CrossRef] [PubMed]
5. Boujibar, O.; Ghamouss, F.; Ghosh, A.; Achak, O.; Chafik, T. Activated carbon with exceptionally high surface area and tailored nanoporosity obtained from natural anthracite and its use in supercapacitors. *J. Power Sources* **2019**, *436*, 226882. [CrossRef]
6. Wu, Y.-C.; Ye, J.; Jiang, G.; Ni, K.; Shu, N.; Taberna, P.-L.; Zhu, Y.; Simon, P. Electrochemical Characterization of Single Layer Graphene/Electrolyte Interface: Effect of Solvent on the Interfacial Capacitance. *Angew. Chem.* **2021**, *133*, 13429–13434. [CrossRef]
7. Miller, E.E.; Hua, Y.; Tezel, F.H. Materials for energy storage: Review of electrode materials and methods of increasing capacitance for supercapacitors. *J. Energy Storage* **2018**, *20*, 30–40. [CrossRef]
8. Boujibar, O.; Ghosh, A.; Achak, O.; Chafik, T.; Ghamouss, F. A high energy storage supercapacitor based on nanoporous activated carbon electrode made from Argan shells with excellent ion transport in aqueous and non-aqueous electrolytes. *J. Energy Storage* **2019**, *26*, 100958. [CrossRef]
9. El-Kady, M.F.; Shao, Y.; Kaner, R.B. Graphene for batteries, supercapacitors and beyond. *Nat. Rev. Mater.* **2016**, *1*, 2058–8437. [CrossRef]
10. Olabi, A.G.; Abdelkareem, M.A.; Wilberforce, T.; Sayed, E.T. Application of graphene in energy storage device—A review. *Renew. Sustain. Energy Rev.* **2021**, *135*, 110026. [CrossRef]
11. Xu, B.; Yue, S.; Sui, Z.; Zhang, X.; Hou, S.; Cao, G.; Yang, Y. What is the choice for supercapacitors: Graphene or graphene oxide? *Energy Environ. Sci.* **2011**, *4*, 2826–2830. [CrossRef]
12. Down, M.P.; Rowley-Neale, S.J.; Smith, G.C.; Banks, C.E. Fabrication of Graphene Oxide Supercapacitor Devices. *ACS Appl. Energy Mater.* **2018**, *1*, 707–714. [CrossRef]
13. Dimiev, A.M.; Tour, J.M. Mechanism of Graphene Oxide Formation. *ACS Nano* **2014**, *8*, 3060–3068. [CrossRef] [PubMed]
14. Hummers, W.S.; Offeman, R.E. Preparation of Graphitic Oxide. *J. Am. Chem. Soc.* **1958**, *80*, 1339. [CrossRef]
15. Marcano, D.C.; Kosynkin, D.V.; Berlin, J.M.; Sinitskii, A.; Sun, Z.; Slesarev, A.; Alemany, L.B.; Lu, W.; Tour, J.M. Improved Synthesis of Graphene Oxide. *ACS Nano* **2010**, *4*, 4806–4814. [CrossRef]
16. Chen, J.; Yao, B.; Li, C.; Shi, G. An improved Hummers method for eco-friendly synthesis of graphene oxide. *Carbon* **2013**, *64*, 225–229. [CrossRef]
17. Wei, Y.; Hu, X.; Jiang, Q.; Sun, Z.; Wang, P.; Qiu, Y.; Liu, W. Influence of graphene oxide with different oxidation levels on the properties of epoxy composites. *Compos. Sci. Technol.* **2018**, *161*, 74–84. [CrossRef]
18. Yadav, N.; Lochab, B. A comparative study of graphene oxide: Hummers, intermediate and improved method. *FlatChem* **2019**, *13*, 40–49. [CrossRef]
19. Gaidukevic, J.; Aukstakojyte, R.; Navickas, T.; Pauliukaite, R.; Barkauskas, J. A novel approach to prepare highly oxidized graphene oxide: Structural and electrochemical investigations. *Appl. Surf. Sci.* **2021**, *567*, 150883. [CrossRef]

20. Botas, C.; Álvarez, P.; Blanco, C.; Santamaría, R.; Granda, M.; Ares, P.; Rodríguez-Reinoso, F.; Menéndez, R. The effect of the parent graphite on the structure of graphene oxide. *Carbon* **2012**, *50*, 275–282. [CrossRef]
21. Sieradzka, M.; Ślusarczyk, C.; Fryczkowski, R.; Janicki, J. Insight into the effect of graphite grain sizes on the morphology, structure and electrical properties of reduced graphene oxide. *J. Mater. Res. Technol.* **2020**, *9*, 7059–7067. [CrossRef]
22. Zhang, S.; Zhao, K.; Zhao, J.; Liu, H.; Chen, X.; Yang, J.; Bao, C. Large-sized graphene oxide as bonding agent for the liquid extrusion of nanoparticle aerogels. *Carbon* **2018**, *136*, 196–203. [CrossRef]
23. Lin, S.; Dong, L.; Zhang, J.; Lu, H. Room-Temperature Intercalation and ~1000-Fold Chemical Expansion for Scalable Preparation of High-Quality Graphene. *Chem. Mater.* **2016**, *28*, 2138–2146. [CrossRef]
24. Dong, L.; Chen, Z.; Lin, S.; Wang, K.; Ma, C.; Lu, H. Reactivity-Controlled Preparation of Ultralarge Graphene Oxide by Chemical Expansion of Graphite. *Chem. Mater.* **2017**, *29*, 564–572. [CrossRef]
25. Liu, Y.; Wu, X.; Tian, Y.; Zhou, X.; Yu, B.; Zhang, Q.; Du, R.; Fu, Q.; Chen, F. Largely enhanced oxidation of graphite flakes via ammonium persulfate-assisted gas expansion for the preparation of graphene oxide sheets. *Carbon* **2019**, *146*, 618–626. [CrossRef]
26. Brunauer, S.; Emmett, P.H.; Teller, E. Adsorption of Gases in Multimolecular Layers. *J. Am. Chem. Soc.* **1938**, *60*, 309–319. [CrossRef]
27. Seaton, N.A.; Walton, J.P.R.B.; Quirke, N. A new analysis method for the determination of the pore size distribution of porous carbons from nitrogen adsorption measurements. *Carbon* **1989**, *27*, 853–861. [CrossRef]
28. Patterson, A.L. The Scherrer Formula for X-Ray Particle Size Determination. *Phys. Rev.* **1939**, *56*, 978–982. [CrossRef]
29. Ferrari, A.C.; Robertson, J. Interpretation of Raman spectra of disordered and amorphous carbon. *Phys. Rev. B* **2000**, *61*, 14095–14107. [CrossRef]
30. Dikin, D.A.; Stankovich, S.; Zimney, E.J.; Piner, R.D.; Dommett, G.H.B.; Evmenenko, G.; Nguyen, S.T.; Ruoff, R.S. Preparation and characterization of graphene oxide paper. *Nature* **2007**, *448*, 457–460. [CrossRef]
31. Rouquerol, J.; Avnir, D.; Fairbridge, C.W.; Everett, D.H.; Haynes, J.M.; Pernicone, N.; Ramsay, J.D.F.; Sing, K.S.W.; Unger, K.K. Recommendations for the characterization of porous solids (Technical Report). *Pure Appl. Chem.* **1994**, *66*, 1739–1758. [CrossRef]
32. Ramesh, P.; Amalraj, S.; Arunachalam, P.; Gopiraman, M.; Al-Mayouf, A.M.; Vasanthkumar, S. Covalent intercalation of hydrazine derived graphene oxide as an efficient 2D material for supercapacitor application. *Synth. Met.* **2021**, *272*, 116656. [CrossRef]
33. Aliyev, E.; Filiz, V.; Khan, M.M.; Lee, Y.J.; Abetz, C.; Abetz, V. Structural Characterization of Graphene Oxide: Surface Functional Groups and Fractionated Oxidative Debris. *Nanomaterials* **2019**, *9*, 1180. [CrossRef] [PubMed]
34. Farivar, F.; Yap, P.L.; Karunagaran, R.U.; Losic, D. Thermogravimetric Analysis (TGA) of Graphene Materials: Effect of Particle Size of Graphene. *Graphene Oxide Graph. Therm. Parameters C* **2021**, *7*, 41.
35. Augustyn, V.; Simon, P.; Dunn, B. Pseudocapacitive oxide materials for high-rate electrochemical energy storage. *Energy Environ. Sci.* **2014**, *7*, 1597–1614. [CrossRef]
36. Antink, W.H.; Choi, Y.; Seong, K.; Kim, J.M.; Piao, Y. Recent Progress in Porous Graphene and Reduced Graphene Oxide-Based Nanomaterials for Electrochemical Energy Storage Devices. *Adv. Mater. Interfaces* **2018**, *5*, 1701212. [CrossRef]
37. Sun, D.; Yan, X.; Lang, J.; Xue, Q. High performance supercapacitor electrode based on graphene paper via flame-induced reduction of graphene oxide paper. *J. Power Sources* **2013**, *222*, 52–58. [CrossRef]
38. Patil, S.M.; Shingte, S.R.; Karade, V.C.; Kim, J.H.; Kulkarni, R.M.; Chougale, A.D.; Patil, P.B. Electrochemical performance of magnetic nanoparticle-decorated reduced graphene oxide (MRGO) in various aqueous electrolyte solutions. *J. Solid State Electrochem.* **2021**, *25*, 927–938. [CrossRef]
39. Hsieh, C.-T.; Hsu, S.-M.; Lin, J.-Y.; Teng, H. Electrochemical Capacitors Based on Graphene Oxide Sheets Using Different Aqueous Electrolytes. *J. Phys. Chem. C* **2011**, *115*, 12367–12374. [CrossRef]
40. Liu, Y.; He, D.; Wu, H.; Duan, J.; Zhang, Y. Hydrothermal Self-assembly of Manganese Dioxide/Manganese Carbonate/Reduced Graphene Oxide Aerogel for Asymmetric Supercapacitors. *Electrochim. Acta* **2015**, *164*, 154–162. [CrossRef]
41. Xu, Y.; Sheng, K.; Li, C.; Shi, G. Self-Assembled Graphene Hydrogel via a One-Step Hydrothermal Process. *ACS Nano* **2010**, *4*, 4324–4330. [CrossRef] [PubMed]